Chapter 3

Intermittency in ^{32}S-Ag/Br interaction at 200A GeV/c

The nature of dynamical fluctuation in the density distribution of singly charged particles produced in ^{32}S-Ag/Br interactions at an incident momentum of 200A GeV/c, has been investigated. The data were collected with the help of nuclear photographic emulsion technique. Different statistical methods of multiplicity moments have been used to analyze this data in terms of the intermittency and fractal properties. The analysis have been performed both in one and two dimensional phase-space distributions. Wherever possible, our experimental results have been compared with the results obtained in similar other heavy-ion induced experiments, as well as with those obtained from simulated events. The investigation shows presence of weak intermittency in one dimension (1-d), which is consistent with self-similarity of the fluctuations. In two dimension (2-d), a kind of anisotropy in the distributions between longitudinal and transverse phase-space variables has been observed. This indicates that, self-affinity rather than self-similarity in the distributions, is responsible for the observed anisotropic behavior. From the analysis of the factorial correlators and oscillatory multiplicity moments, presence of a few particle short ranged correlation has also been established. In almost all cases, the simulated interactions failed to replicate the experimental results.

3.1 Introduction

The single particle phase-space distribution of charged particles produced in a high-energy interaction exhibits rapid fluctuations that contain spikes as well as dips. Such fluctuations have two different origins. One comes from the statistical noise due to finite multiplicity of particles in an event, and the other comes from some nontrivial dynamical reason that can not be directly measured in an experiment. When the density function is averaged over an entire sample of events, the effect of statistical noise can be substantially reduced. But at the same time the dynamical part of these fluctuations is also averaged out, resulting in a smooth distribution of the final state hadrons. The method of analyzing multiparticle data underwent a paradigm shift when Bialas and Peschanski first suggested that, the particle density function should be examined locally within narrow regions of phase-space [1], and they themselves applied the technique of scaled factorial moment (SFM) on the now famous JACEE events induced by ultra high-energy cosmic ray nuclei [2]. The SFMs of integer order were found to depend on the phase-space resolution obeying a power law scaling behaviour. Such a scaling behaviour of the SFM has since then been known as 'intermittency'. During last two decades or so, the topic has generated quite a significant amount of research interest within and beyond the high-energy physics community, and a whole range of new issues related to the complex process of multiparticle production have opened up. Experiments have been performed with different types of colliding particles that also involve widely varying values of collision energy. Various other methods have been proposed to identify the extent and nature of fluctuations, so that the mechanism of particle production can be understood within the framework of existing models. A large section of these techniques is based on the notion that, the density distribution of produced particles has a self-similar or fractal nature, that may have resulted due to some kind of scale invariant dynamics. Similar to the SFM, several other moments of density distribution have been found to depend on the phase-space interval size obeying different types of power laws, that indicates possibility of a fractal structure in the underlying distribution. Efforts have been made to interpret the observed scale invariance of moments of particle density distribution in terms of the random cascading model, phase transition or more conventional mechanisms like the cluster production or Bose-Einstein correlation etc. Both the experimental and phenomenological status of the subject has been compre-

hensively reviewed by De Wolf, Dremin and Kittel [3].

In this chapter we are going to present an analysis of a data set on the angular emission of singly charged secondary particles produced in central and semicentral ^{32}S-Ag/Br interactions at an incident momentum of 200 A GeV/c. Centered around two basic ideas of self-similarity and self-affinity of density fluctuation, the scaling behaviour of different types of multiplicity moments as functions of phase-space interval size, has been examined. As far as possible, efforts have been made to correlate the results obtained from different techniques of data analysis. For the purpose of comparison, whenever felt necessary, references of similar other heavy-ion induced experiments have been made. Results obtained by analyzing simulated ^{32}S-Ag/Br events at the same incident momentum and having identical multiplicity distribution as the experimental one, have been incorporated. The major objectives of the present investigation are, (i) to study the intermittency phenomenon of multiparticle production in 1-d and 2-d, (ii) to examine whether the intermittency is a result of self-similarity or self-affinity in the branching (cascading) process, (iii) to compare the experimental results with at least one of the extensively used models of particle production in high-energy AB interactions, and lastly (iv) to identify the influence of particle correlation in the observed intermittent behaviour.

3.2 Methodology and Results

As mentioned above, a high-energy AB interaction contains rapidly fluctuating particle density in different regions of phase-space, that gets smoothed out when averaged over many events. In Fig. 3.1(a) and (b) the η distribution of two high multiplicty ^{32}S-Ag/Br interactions at 200A GeV/c incident momentum, with interval size $\delta\eta = 0.2$ have been schematically presented. In Fig. 3.1(c) and (d) the same plots are made with a reduced interval size, $\delta\eta = 0.1$, and the extent of fluctuations drastically increases. The presence of both peaks and dips has been highlighted by drawing Gaussian fits to the data. When averaged over many events, these local fluctuations are smoothed out, as can be seen from the plot of $N_{ev}^{-1}\,(dn_s/d\eta)$ against η in Fig. 2.3(a). Distribution of these local densities $dn_s/d\eta$ obtained from individual events can be found in Fig. 3.2(a) and (b). These

distributions correspond only to the central particle producing region, respectively, to $\eta_0 \leq \eta < \eta_0 + 1$ and $\eta_0 - 1 < \eta \leq \eta_0$, where η_0 is the peak position of the Gaussian fit shown in Fig. 2.3(a), and the density values are obtained with $\delta\eta = 0.2$. In these diagrams $dn_s/d\eta$ values as large as ~ 150 can be observed.

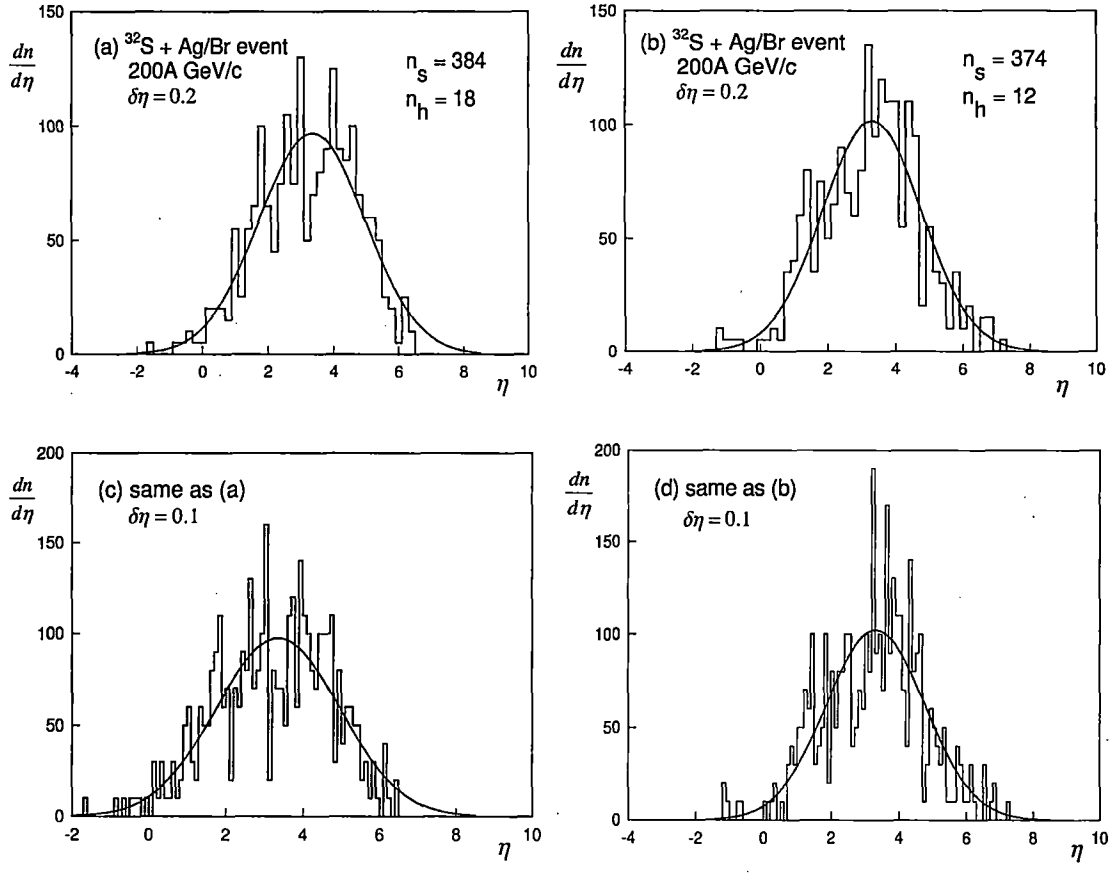

Figure 3.1: Pseudorapidity distribution of shower tracks of two high multiplicity ^{32}S-Ag/Br events. (a) and (b) with $\delta\eta = 0.2$; (c) and (d) with $\delta\eta = 0.1$. Note how the fluctuation increases with decreasing bin size. Solid curves represent Gaussian fits to the data.

Dynamical fluctuation of produced particles can be analyzed in terms of the factorial moments (f_q). The q-th order (q is a positive integer) factorial moment is defined as,

$$f_q = n_j\,(n_j - 1)\,....\,(n_j - q + 1),$$

where n_j is the particle number falling in the jth phase-space interval of an event. The entire range of phase-space say (ΔX), has been divided into M intervals of equal size say $\delta X = \Delta X/M$. If the phase-space distribution $P(n)$ of the particle multiplicity (n) is considered as a convolution of a dynamical part $D(\xi)$ and a Poisson type statistical part,

$$P(n) = \int dt \frac{t^n e^{-t}}{n!} D(t),$$

then summing over n the event averaged factorial moment $< f_q >$ is given by,

$$< f_q > = \sum_q^\infty \frac{n!}{(n-q)!} P(n) = \int dt\, t^q\, D(t).$$

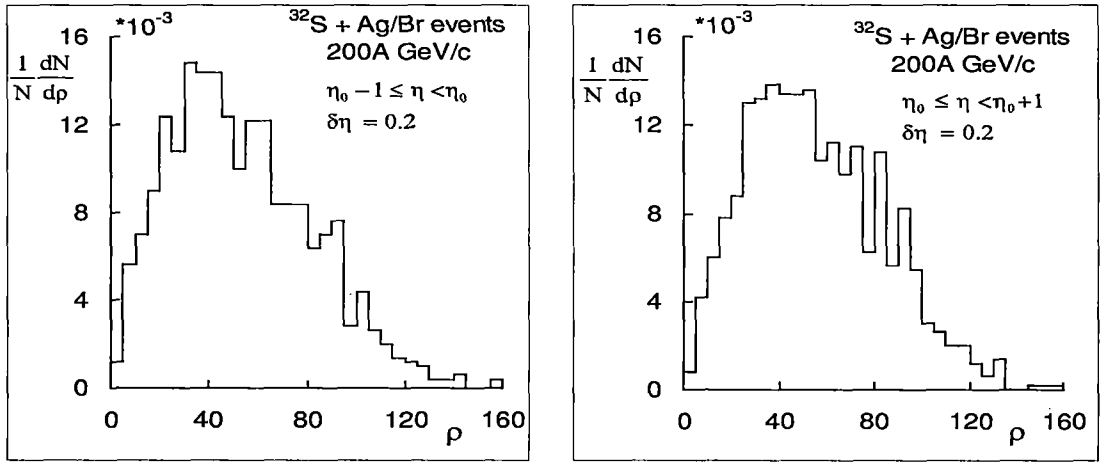

Figure 3.2: Distribution of local density of particles produced in ^{32}S-Ag/Br interactions at 200A GeV/c. The η range and size of $\delta\eta$ are shown in each diagram.

Hence one can see that the event averaged factorial moment is nothing but the simple moment of the corresponding dynamical part of the phase-space distribution, irrespective of the exact analytical form of the dynamical component. Thus $< f_q >$ are capable of suppressing the Poisson type statistical noise, which the ordinary moments can not. This kind of noise suppression is not possible, (i) if n does not tend to ∞, or (ii) the statistical part is not of Poisson type. Fortunately in our sample of high-energy AB collision, $n \rightarrow$ a large value, and the Poisson nature of statistical fluctuation in bin multiplicity could also be confirmed by generating random numbers. Note that bins only with $n_j \geq q$ contribute to f_q, but f_q is not sensitive to the position of the bin. However, in the case of AB collision

where average multiplicity is large, many bins contribute if the order is not too large or the bin width is not too low. Hence the bin position is not so important. f_q can not only measure large scale fluctuations, but as we shall find later, they can also provide information about the pattern of these fluctuations. The f_q values can be normalized (or scaled) by the global average multiplicity of particles ($< n_s >$ in the present case), and such a normalized moment is called the SFM. Averaged over an event sample, the SFM of order q is denoted by $< F_q >$ and is therefore, defined as [1],

$$< F_q >_h = \frac{1}{N_{ev}} \sum_{i=1}^{N_{ev}} M^{q-1} \sum_{j=1}^{M} \frac{n_{ij}(n_{ij}-1)....(n_{ij}-q+1)}{< n_s >^q}, \tag{3.1}$$

where

$$< n_s > = \frac{1}{N_{ev}} \sum_{i=1}^{N_{ev}} n_s,$$

and n_{ij} is the number of particles falling into the jth such interval of the ith event. In the above definition of $< F_q >_h$, the so called 'horizontal' averaging method has been adopted. The SFM defined in this way is sensitive to the shape of the single particle distribution, and it further depends on the correlation between different phase-space intervals. The problem of shape dependence can be solved either by applying the Fialkowski correction factor [5] given by,

$$R_F(q,M) = \frac{1}{M} \sum_{j=1}^{M} M^q \frac{< n_j >^q}{< n_s >^q} : \quad < n_j > = \frac{1}{N_{ev}} \sum_{i=1}^{N_{ev}} n_{ij},$$

or by replacing the phase-space variable (say η) with a cumulative variable X_η defined as [6],

$$X_\eta = \left[\int_{\eta_{min}}^{\eta} \rho(\eta) d\eta \right] / \left[\int_{\eta_{min}}^{\eta_{max}} \rho(\eta) d\eta \right].$$

Here, $\eta_{min}(\eta_{max})$ is the minimum (maximum) value of η, and $\rho(\eta)$ is the single particle density function in terms of η. Irrespective of the basic phase-space variable from which it is derived, the X distribution is always uniform within $0 \leq X \leq 1$. Though our entire analysis on multiplicity moments will henceforth be preformed by considering X_η and/or X_φ as the phase-space variables, we shall continue to call the corresponding space either the η-space or the φ-space. The problem of correlation between different intervals can be eliminated by considering the so called 'vertical' averaging of the SFM that is locally

normalized by the average bin multiplicity. They carry information about the event space fluctuations within each interval, and are defined as,

$$< F_q >_v = \frac{1}{M} \sum_{m=1}^{M} \frac{1}{N_{ev}} \sum_{i=1}^{N_{ev}} \frac{n_{ij}(n_{ij}-1)....(n_{ij}-q+1)}{< n_j >^q}. \tag{3.2}$$

In case of particle production the term 'intermittency' is not used in the strict hydrodynamical sense from where the word has been coined, but it refers only to a scale invariance of the SFM with decreasing size of the phase-space interval δX, abiding a power law such as,

$$< F_q(\delta X) > \propto (\delta X)^{-\phi_q} : \quad \delta X \to 0. \tag{3.3}$$

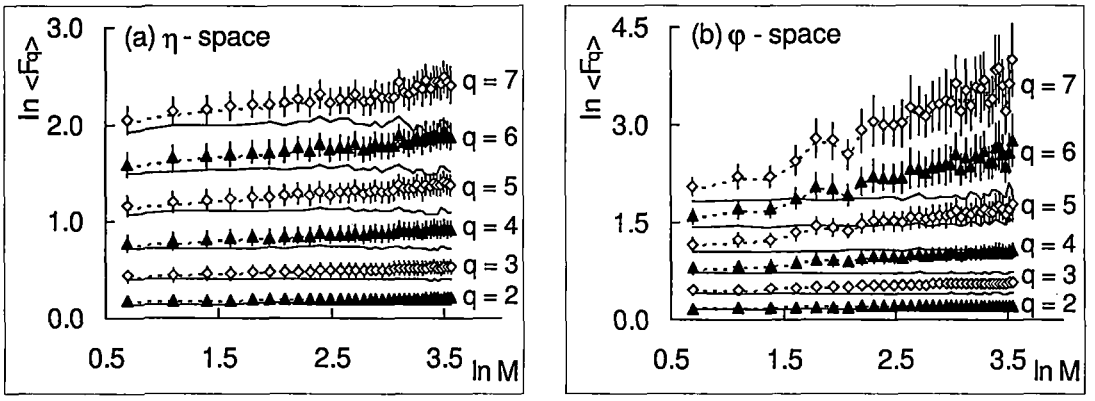

Figure 3.3: Variation of SFM of different orders with phase-space partition number. In both (a) and (b) the points represent experimental values of horizontally averaged moments, and the dotted lines are obtained by connecting the experimental values of vertically averaged moments. Whereas in (a) the solid lines are obtained by joining the FRITIOF simulated values of horizontally averaged SFM, in (b) the soild lines correspond to those obtained by generating random numbers.

In Fig. 3.3(a) our results on intermittency analysis in the η-space have been graphically plotted along with the corresponding FRITIOF predictions. The error bar associated with each experimental $< F_q >_h$ value is merely of statistical origin. They have been estimated by assuming that F_q for each event is an error free quantity, and thus the correlation between different phase-space intervals has been ignored. The average multiplicity for the present sample of events is substantially high, and therefore, this simplification in error estimation is not going to significantly influence our results [7]. Both the horizontally and

vertically averaged SFM have been calculated with respect to the uniformly distributed cumulative variable X_η, and for any q no significant difference in the values from two different averaging methods could be seen. For all orders linear rise in $\ln < F_q >$ values with increasing $\ln M$ as given by Eq. (3.3), can be observed in our experimental results. This trend is missing in the corresponding FRITIOF predictions. Similar plot in the φ-space can be found in Fig. 3.3(b). Due to conservation of linear momentum, particles tend to move in opposite directions in a plane transverse to the incident projectile direction. Due to this effect $< F_q >$ values obtained for small values of partition number in the φ-space, do not follow the same linear trend as that in the large M region, where such effects of kinematic conservation laws get reduced. Therefore, in this case for each q, the first four experimental data points corresponding to the smaller values of $M\,(< 6)$ have been excluded from the process of straight line fit. SFM values have also been computed by generating random numbers distributed uniformly over an interval of $(0, 1)$, and for comparison these values are incorporated in Fig. 3.3(b). As expected, the $< F_q >$ values obtained from random numbers do not exhibit any rise. They remain more or less uniformly distributed with decreasing bin size.

The exponents ϕ_q, called intermittency indices, possess positive values, and each should be a constant for any given order q. These indices are obtained from the slopes of best fitted straight lines of $\ln < F_q >$ vs. $\ln M$ data. For both η and φ-spaces, the experimentally obtained intermittency indices are given in Table 3.1. Values of Pearson's r^2 coefficient [8], showing goodness of linearity in the $\ln M$ dependence of $\ln < F_q >$, are also given in Table 3.1. In almost all cases the r^2 values are close to $+1$, confirming the validity of the power law scaling behavior of the SFM as given in Eq. (3.3). In φ-space the intermittency indexes are consistently higher than those in η-space, indicating that in our case intermittency analysis is not independent of the phase-space variable considered. At this point it should be mentioned that, for a given order the data points in Fig. 3.3 are highly correlated, because the SFM are computed for the same sample of events with differing bin size. The error estimation of ϕ_q is therefore, an extremely different task. For this purpose we have adopted the method of simulating several independent event samples, each of same size and having identical multiplicity distribution as the experimental one, and have obtained ϕ_q for each such sample [9]. The errors associated with the ϕ_q values

shown in Table 3.1 are nothing but the standard deviation of different ϕ_q values obtained from ten such independently simulated event samples,

$$\sigma(\phi_q) = \sqrt{< \phi_q{}^2 > - < \phi_q >^2},$$

where <> indicates averaging over the number of event samples generated. The FRITIOF code has been used for the η-space, whereas random numbers have been used for the φ-space. As neither the FRITIOF nor the random number generated samples can account for the dynamical intermittency effect, the errors evaluated through this indirect method are obviously underestimated.

Table 3.1 Intermittency indices for experimental and simulated data sets along with Pearson's r^2 values indicating the goodness of fit.

Order	η - space		φ - space	
	ϕ_q	r^2	ϕ_q	r^2
q=2	0.013 ±0.003	0.982	0.014 ±0.0006	0.967
q=3	0.032 ±0.003	0.977	0.044 ±0.002	0.972
q=4	0.056 ±0.007	0.961	0.099 ±0.005	0.967
q=5	0.082 ±0.013	0.937	0.201 ±0.011	0.946
q=6	0.112 ±0.021	0.905	0.371 ±0.021	0.915
q=7	0.138 ±0.033	0.865	0.607 ±0.039	0.888

Due to intermixing of many sources of particle production, the intermittency indexes ϕ_q in ^{32}S-Ag/Br interactions at 200A GeV/c are smaller than those in the leptonic [10] and hadronic collisions [7] at comparable energies, but they are comparable to similar AB experiments [11]. To examine whether or not the observed intermittency effect is exclusively a result of the contribution from lower order correlation functions, the normalized exponents

$$\zeta_q = \phi_q / \binom{q}{2}, \tag{3.4}$$

with $q \geq 2$ are evaluated. True three particle correlation in terms of these normalized slopes can be written as,

$$\zeta_q^{(3)} = (q-2)\zeta_3 - (q-3)\zeta_2. \tag{3.5}$$

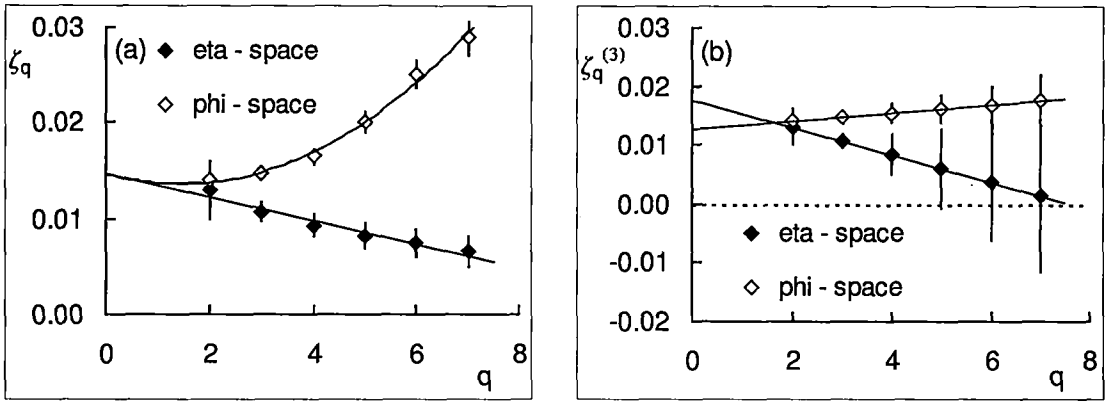

Figure 3.4: Normalized intermittency exponents plotted against q for the experimental data. The straight lines and the quadratic curve are best fit to data.

Variation of both types of experimentally obtained normalized exponents against q are graphically represented in Fig. 3.4(a) and (b), respectively for η-space and φ-space. A linear variation of ζ_q with q can be observed for the η-space, whereas, in the φ-space the behavior is not linear. In neither case normalized slopes are independent of q. The difference in behaviour in η and φ-spaces can also be seen from the variation of $\zeta_q^{(3)}$ with q, while one decreases with q, the other increases. From this analysis it can not be unambiguously concluded that all correlations for $q \geq 4$, particularly in the φ-space, can be explained only in terms of two and three-particle correlations.

The order (q) dependence of intermittency index ϕ_q can be further used to look into different probable mechanisms of particle production. It has been pointed out that, intermittency as scale invariance of SFM may be observed either due to a branching process, or due to some kind of phase transition [12]. Whereas, multiplicative cascade models based on the branching process exhibit a multifractal structure, a second order phase transition as another possible mechanism of particle production, will lead to monofractal pattern in the fluctuation of final state particles. Multifractality, as a possible reason for intermittency, is connected to an infinite number of anomalous dimensions $d_q(= D - D_q)$, which are again directly related to the intermittency indexes ϕ_q as,

$$d_q = \phi_q/(q-1). \tag{3.6}$$

Here D_q is the generalized qth order Renyi dimension, and D is the ordinary topological dimension of the space into which the fractal objects are embedded. For a self-similar

cascade mechanism the probability density distribution is obtained by using the Levy stable law, that is characterized by a Levy stability index μ considered to be a measure of the degree of multifractality. Under the Levy-law approximation [14], the ratio of anomalous dimensions is expected to follow a relation like,

$$\frac{d_q}{d_2} = \frac{1}{2^{\mu} - 2} \frac{(q^{\mu} - q)}{(q-1)}. \tag{3.7}$$

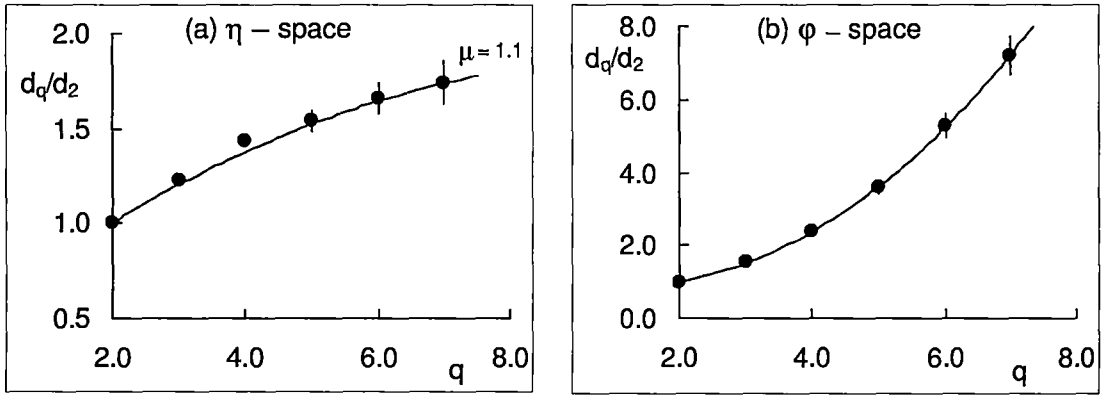

Figure 3.5: (a) Plot of $\frac{d_q}{d_2}$ against q in η-space. The solid line represents corresponding values of $\frac{d_q}{d_2}$ obtained from Eq. (3.7) with $\mu = 1.1$. (b) Plot of $\frac{d_q}{d_2}$ against q in φ-space. The solid line has been drawn just to guide the eye.

In Fig. 3.5 our results on the anomalous dimensions obtained from intermittency analysis have been graphically shown. Whereas, in η-space the ratio d_q/d_2 slowly increases with q, the same in φ-space clearly exhibits a quadratic increase. The behaviour of anomalous dimensions in φ-space is not in conformity with the prediction of Levy-law. Therefore, the Levy index is obtained only for the η-space and it came out to be $\mu = 1.1$. This value is less than a previously obtained value ($\mu = 1.6$) in high-energy pA and heavy-ion interaction [12], but is still within the limit allowed by the Levy-law $0 \leq \mu \leq 2$, and is indicative of a wild singularity in the multifractal structure. The spiky structure of density distribution of particles can be also examined with the help of a set of bunching parameters [13]. In this approach, higher order bunching parameters can be expressed in terms of the lower order parameters, resulting in a linear expression like,

$$d_q = d_2\,(1 - r) + \frac{q}{2}\, d_2\, r. \tag{3.8}$$

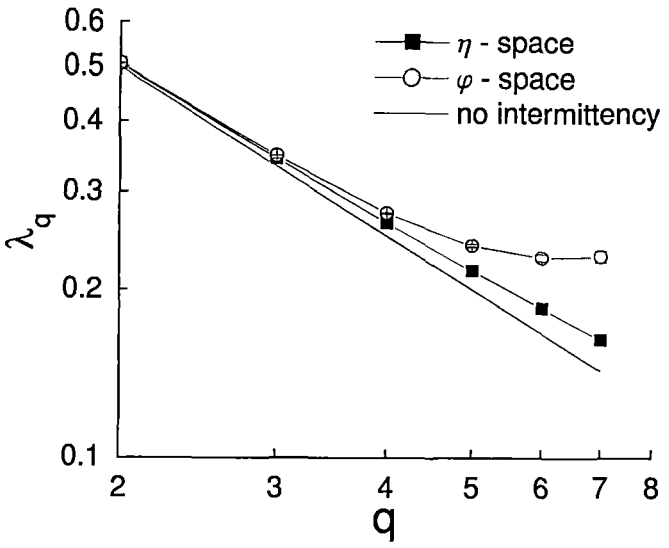

Figure 3.6: Plot of λ_q against q. The no-intermittency line corresponding to $\phi_q = 0$ has also been shown.

A nonzero value of the slope r implies a multifractal behaviour, and in η-space it came out to be $r = 0.383 \pm 0.015$. Note that if $\mu = 0$, $d_q = d_2$, and the multifractal behaviour reduces to a monofractal behaviour. It has been mentioned earlier that, such a condition would have indicated in favour of a possible phase transition, which the intermittency analysis of present set of heavy-ion data does not. It is probably still worthwhile to give a closer look into this aspect and examine different possibilities for the observed intermittency. On the basis of the Ginzburg-Landau (GL) theory it has been predicted that [15], a thermal phase transition may be a reason for intermittency, where a universal parameter ν describes the variation of d_q as,

$$\frac{d_q}{d_2} = (q-1)^{(\nu-1)}. \tag{3.9}$$

In the present case it has been found that, $\nu = 1.327 \pm 0.009$ for the η-space. In comparison with other heavy-ion results, within statistical errors ν in the present experiment is closer to the universal value $\nu = 1.304$, as it should be for all systems describable by the GL theory [3]. However, because d_q values are obtained from ϕ_q, and the errors in ϕ_q are underestimated as they do not contain any contribution from the dynamical fluctuation, therefore, one should be extra cautious while trying to draw any conclusion about the

underlying physical process. Occurrence of a nonthermal phase transition is another possibility, where intermittency can be observed as a result of a parton-shower cascading process, and different phases can coexist if the function,

$$\lambda_q = \frac{\phi_q + 1}{q}, \tag{3.10}$$

exhibit a minimum at a certain critical value $\lambda_q = \lambda_c$ [16]. Behaviour of λ_q as a function of q has been presented in Fig. 3.6, where no such minimum can be observed. Small deviations of experimental results from the 'no intermittency' line ($\phi_q = 0$) indicate only a presence of weak intermittency in the one dimensional analysis of our data. It may be noted however, that the deviation is larger in φ-space than in the η-space.

3.2.1 Intemittency in 2-d

In 1-d the intermittency effect has not been found to be very prominent. The SFM technique can therefore be extended to the two dimensional $(\eta - \varphi)$ plane, to examine whether or not the so called 'projection effect' is responsible for the observed weak intermittency in 1-d. The entire range of each cumulant variable $0 \leq X_\eta, (X_\varphi) \leq 1$, has been partitioned into M_1 intervals of equal size, resulting in a total of $M = (M_1)^2$ such intervals of the 2-d plane. Making use of Eq. (3.1) the SFM are now evaluated. In Fig. 3.7 these 2-d moments have been plotted against the partition number M. The variation of $\ln < F_q >$ in 2-d is clearly not linear over the entire range of $\ln M$. For each q an upward bending in the variation of $\ln < F_q >$ with $\ln M$ can be seen. For $q = 4$ and 5 probably due to finite shower multiplicity, one can see saturation effects in large $\ln M$ region. In 2-d partition most of the events do not contribute to F_6 or F_7. Therefore, these moments have not been calculated. Obtaining ϕ_q from such nonlinear dependence does not carry any meaning, as the value will depend on the region where the linear fit has been performed. However, within a restricted $\ln M$ region (for $400 \geq M \geq 64$), linear fit of the data has resulted in the following indexes, $\phi_2^2 = 0.075 \pm 0.003$, $\chi^2(dof) = 0.17(11)$; $\phi_3^2 = 0.384 \pm 0.038$, $\chi^2(dof) = 0.79(11)$; $\phi_4^2 = 1.03 \pm 0.17$, $\chi^2(dof) = 2.27(11)$; $\phi_5^2 = 1.56 \pm 0.29$, $\chi^2(dof) = 4.48(11)$. The superscript 2 associated with each ϕ_q denotes the dimensionality of phase-space. The ratio of 2-d and 1-d intermittency exponents for $q = 2$ is, $\phi_2^2/\phi_2 \approx 6$, which is consistent with the previously obtained results from similar heavy-ion experiments [11]. On the other hand,

in contrast to the finding of [11], the ratio ϕ_q/ϕ_2 in the present case is not found to be a dimension independent quantity.

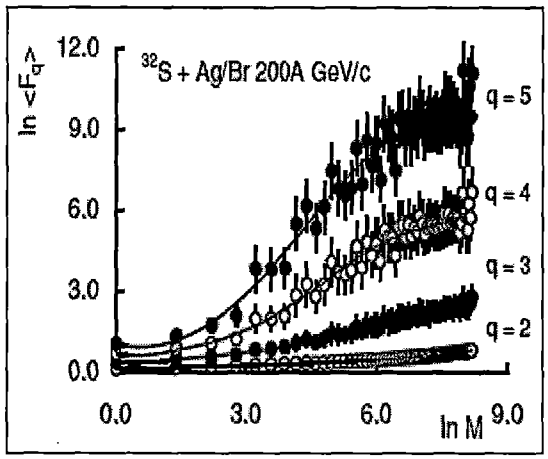

Figure 3.7: Plot of 2-d SFM of different order against phase-space partition number. The lines are drawn to guide the eye.

The issue of electron pairs produced through γ-conversion or otherwise, as being responsible for the observed intermittency effect has been addressed by the EMU01 collaboration. In a 1-d intermittency analysis of ^{32}S-Emulsion data they have found that, the contribution of electron pairs do not significantly influence the observed intermittency effects, whereas in 2-d their intermittency signal is hidden in the background from γ-conversion [9]. Most of the electron pair tracks in EMU01 experiment with vertically irradiated emulsion films have originated from their Au-foil targets. We would like to mention that in the present case, Ag ($Z = 47$) or Br ($Z = 37$) nuclei have the highest atomic no. among the target nuclei. Even their Z-values are smaller than Au ($Z = 79$). Therefore, the rate of γ-conversion, which is a function of Z^2, would be considerably smaller in our case. Moreover, the electron pair tracks produced through γ-conversion, emanate not from the interaction vertex, but are produced at a distance from the vertex after traveling through certain radiation lengths. While scanning horizontally exposed plates, with experienced eye such tracks can be distinguished from the tracks coming out of the point of interaction, and have therefore, been excluded from our consideration of shower tracks. Such a process of filtering out electron pair tracks is difficult in horizontally exposed emulsion

films. It would not be improper to mention that, as observed in a different occasion by the same collaboration [21], the nuclear effects on intermittency can certainly be a topic of investigation, irrespective of their physical origin.

It has been argued that [17], multiparticle production in high-energy interactions is an anisotropic process. Whereas, the longitudinal momenta can vary over a wide range, the transverse momenta are limited within a short range of values with a universal average of $< p_t > \approx 0.35$ GeV/c only. The observed nonlinearity in the 2-d analysis of SFM is a result of this asymmetry. If a QGP like state is formed in an AB collision, their will not be any elementary NN collision, and the entire AB system will thermalize to melt into a unique system. Under such a situation upward bending of the 2-d SFM may not be observed. But under ordinary circumstances, an AB collision can be looked upon as a superposition of many elementary NN collisions, η centers of which are generally distributed over the η-axis. When the entire η range $\Delta\eta(= \eta_{max} - \eta_{min})$ of each NN interaction is divided into M equal partitions, the effective bin size for the AB process actually becomes $< \Delta\eta/M$. Because of the restriction $0 \leq \varphi \leq 2\pi$ the situation in φ-space is different. Hence the usual practice of dividing a 2-d anisotropic phase-space into subcells of equal size, a method compatible to the self-similar fractal property, will not result into same scaling behaviour of the SFM in the longitudinal (η) as well as in the transverse (φ) directions [18]. When the pattern of fluctuations scale in different ways in different directions of phase-space, it is a characteristic of a self-affine fractal, rather than a self-similar one. This kind of self-affinity in nonstatistical fluctuation can be investigated by shrinking the phase-space interval size in two anisotropic independent directions in different ways, e.g.,

$$\begin{aligned} M_\varphi = M_\eta^H : \qquad & M_\eta = 2, 3, ..., 60; \qquad H < 1.0 \\ M_\eta = M_\varphi^{(1/H)} : \qquad & M_\varphi = 2, 3, ..., 60; \qquad H > 1.0. \end{aligned} \tag{3.11}$$

Here M_η (M_φ) is the partition number of the η (φ) space. The new parameter H is called the Hurst exponent, and it is a measure of the self-affine property of the fractal structure. Eq. (3.11) suggests that for $H < 1.0$ the η-space is partitioned into finer intervals, whereas, for $H > 1.0$ the φ-space is partitioned into finer intervals. Obviously if one sets $M_\eta = M_\varphi = M$, the 2-d phase-space is shrunk self-similarly. It is also obvious that, both M_η and M_φ can not be integers, and at least one of them is only a positive real number, say $M = N + a$, where N is an integer and $0 \leq a < 1$. As any one of the 1-d

space is divided into M cells of width $\delta X = 1/M$, N such cells and a smaller one of width a/M are obtained. Replacing M by N in Eq. (3.1) and ignoring the contribution of the smaller cell that is positioned either in front of or after these N cells, one can obtain the SFM in a similar manner as has been done before.

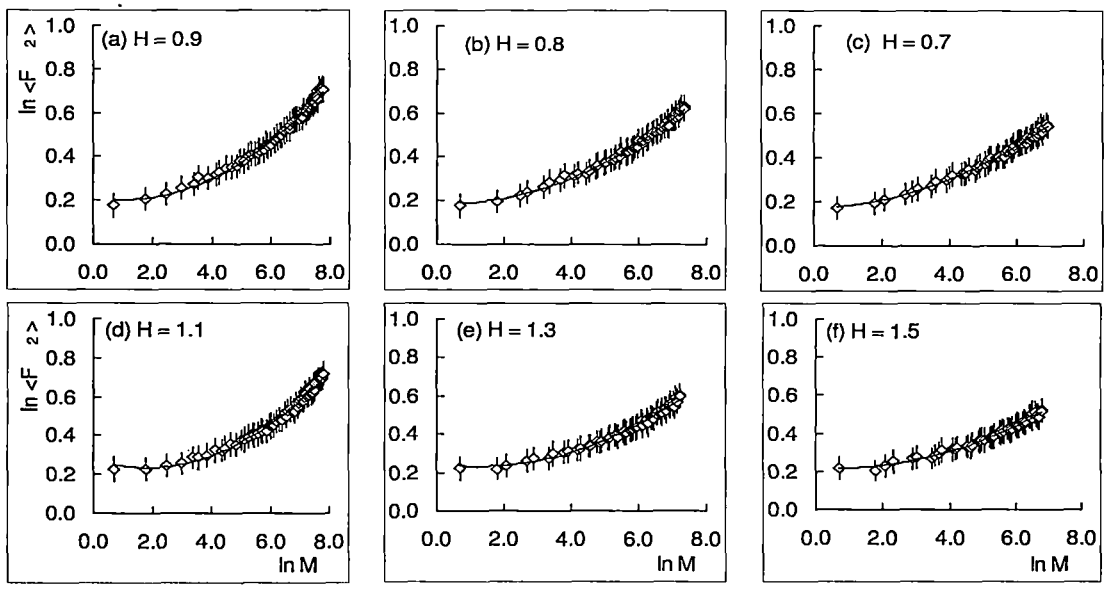

Figure 3.8: Plot of anomalous SFM of order 2 against phase-space partition number in 2-d. The lines represent best fitted quadratic function $f(\xi) = a\,\xi^2 + b\,\xi + c$ of the data.

How the self-affine SFM of second order for different values of H depends on M, has been graphically shown in Fig. 3.8. Whereas Fig. 3.8(a) to 3.8(c) correspond to real M_φ and integer M_η i.e., $H < 1.0$, Fig. 3.8(d) to 3.8(f) correspond to the $H > 1.0$ case. In each case, experimental points are fitted with a quadratic function like $f(\xi) = a\,\xi^2 + b\,\xi + c$, and the values of the fit parameters along with the $\chi^2(dof)$ values showing goodness of fit are presented in Table 3.2. From Fig. 3.8 as well as from the parameter values given in Table 3.2, one can see that, as H deviates more and more from unity, the non-linearity slowly disappears straightening out the $\ln M$ dependence of $\ln < F_2 >$. As H becomes substantially different from unity ($H \approx 0.5$), growing discontinuities in the variation of self-affine $< F_2 >$ are observed. In a similar heavy-ion induced experiment [21] anomalous scaling of SFM was better observed in finer resolutions of η-space than in the φ-space. In

contrast to that, in the present case no such preference of any of the phase-space variables over the other can be established. However, the analysis confirms anisotropy between the distributions of produced particles along the longitudinal variable (η) and the transverse one (φ).

Table 3.2 Values of fit parameters of experimental anomalous moments of $q = 2$ with a quadratic function $f(\xi) = a\,\xi^2 + b\,\xi + c$, along with the χ^2 and number of degrees of freedom showing goodness of fit.

Value of Hurst exponent	Value of a	Value of b	χ^2(d.o.f)
H = 0.6	0.0058 ± 0.00048	0.0107 ± 0.0041	1.893 (57)
H = 0.7	0.0069 ± 0.00042	0.0062 ± 0.0038	1.349 (57)
H = 0.8	0.0089 ± 0.00046	- 0.0071 ± 0.0044	2.055 (57)
H = 0.9	0.0108 ±0.00052	- 0.0224 ± 0.0053	3.259 (57)
H = 1.1	0.0131 ± 0.00057	- 0.0487 ± 0.0059	3.514 (57)
H = 1.2	0.0116 ± 0.00058	- 0.0377 ± 0.0057	2.797 (57)
H = 1.3	0.0098 ± 0.00052	- 0.0249 ± 0.0049	1.947 (57)
H = 1.4	0.0092 ± 0.00057	- 0.0199 ± 0.0052	1.996 (57)
H = 1.5	0.0076 ± 0.00052	- 0.0088 ± 0.0046	1.501 (57)

It should be pointed out that, the methodology to examine self-affinity in phase-space structure, as described in [19] is based on the assumption that, both the probability density and the dynamical fluctuation are uniformly distributed in phase-space. Nonuniformity in either of these distributions may lead to a discontinuity in the variation of the self-affine SFM [20]. Making use of the cumulant variables (X_η, X_φ) the first condition could be achieved in the present case, whereas, the second one could not be achieved as the frequency distributions of the SFM values are nonuniform. Therefore, it can influence our result. Necessary corrective measure as suggested in the case of NA22 results [20], has been employed for $q = 2$ by introducing a correction factor $R(x)$ as,

$$F_2 = \frac{1}{R(x)} \frac{1}{N_{ev}} \sum_{i=1}^{N_{ev}} \frac{1}{N} \sum_{j=1}^{N} \frac{n_{ij}(n_{ij}-1)}{< n >^2}. \tag{3.12}$$

Here $< n >$ is calculated by excluding the contribution of the bin of width a/M. With two integers N' and M', a correction matrix is then introduced as the ratio of the SFM averaged only over N'/M' part of the entire 2-d space,

$$C(N', M') = \frac{\frac{1}{N_{ev}} \sum_{i=1}^{N_{ev}} \frac{1}{N'} \sum_{j=1}^{N'} \frac{n_{ij}(n_{ij}-1)}{<n>^2}}{\frac{1}{N_{ev}} \sum_{i=1}^{N_{ev}} \frac{1}{M'} \sum_{j=1}^{M'} \frac{n_{ij}(n_{ij}-1)}{<n>^2}}. \tag{3.13}$$

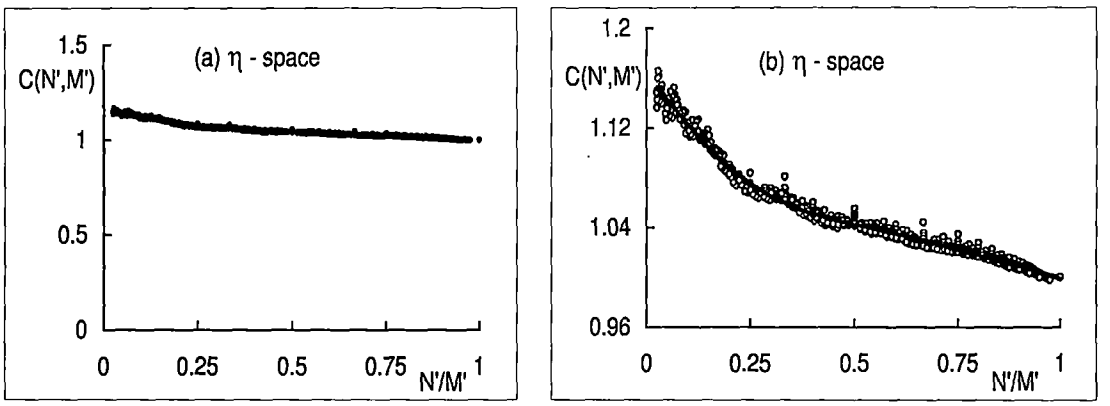

Figure 3.9: Plot of correction factor $C(N', M')$ as a function of N'/M'. Notice the change in scale in two diagrams. Solid curve in (b) represents interpolated polynomial fit.

A plot of this correction matrix for noninteger partition of η-space has been shown in Fig. 3.9. In Fig. 3.9(a) the scale along the abscissa is considerably shrunk and the variation appears as almost linear with a small $(-)$ve gradient. When the same plot is made with a enlarged scale one gets an actual feeling of how nonlinear is the change of $C(N', M')$ with N'/M'. $C(N', M')$ is then supposed to be approximately equal to $R(x)$ if the integers N' and M' are chosen in such a way that,

$$\frac{N'}{M'} \approx \frac{N}{M} = x. \tag{3.14}$$

The factor $R(x) = R(N/M)$ is thereafter, obtained with the help of a polynomial (degree 6) interpolation of the variation of $C(N', M')$ against N'/M'. The solid curve shown in Fig. 3.9(b) represents this polynomial fit of the data. In Fig. 3.10 plots of self-affine SFM $\ln < F_2 >$ at $H = 0.5$ have been shown both before and after making use of the correction factor $R(x)$. Standard errors are associated with the uncorrected data points.

Unfortunately, as one can see from Fig. 3.10 the technique [20] has been found to be inadequate to remove the discontinuities in the variation of ln $< F_2 >$.

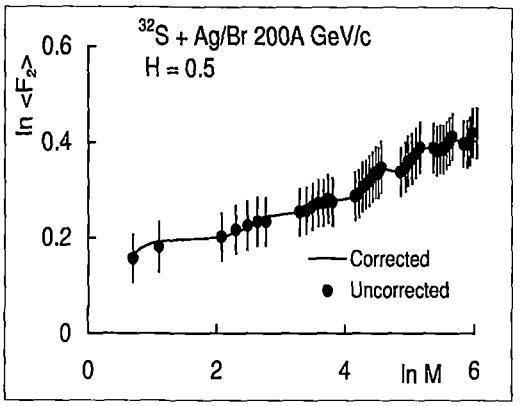

Figure 3.10: Plot of anomalous ln $\langle F_2 \rangle$ against phase-space partition number in 2-d for $H = 0.5$. Solid circles represent uncorrected values, and the continuous curve has been drawn by joining the corresponding corrected values.

3.2.2 Factorial Correlators

Dynamics of particle production beyond that obtained from the single particle inclusive spectra, can be investigated by studying the correlation effects. Whereas, the SFM can be used as a measure of local density fluctuations, the two-fold factorial moments or the factorial correlators [1] denoted by F_{pq}, can extract additional information on the bin to bin correlation between these fluctuations within an event [9, 22]. The factorial correlators are calculated for each combination of nonoverlapping pair of of bins (jj') separated by a fixed distance D. For the sake of statistics they are then averaged over all such combinations of bins. The correlators are defined as,

$$\tilde{F}_{pq} = \frac{< n_j^{[p]} n_{j'}^{[q]} >}{\tilde{F}_p \tilde{F}_q}. \tag{3.15}$$

Here, $n_j^{[q]} = n_j(n_j - 1).....(n_j - q + 1)$, $\tilde{F}_q =< n_j^{[q]} >$, and $n_j(n_{j'})$ is the number of particles in the $j(j')$th bin. As $p \neq q$, $\tilde{F}_{pq}$ as defined in Eq. (3.15) is not symmetric. They are therefore, symmetrized as

$$< F_{pq} >= (\tilde{F}_{pq} + \tilde{F}_{qp})/2. \tag{3.16}$$

According to a simple intermittency model (α-model) [1], F_{pq} should depend on the correlation distance D but not on the interval size δX_η say, and should follow a power law like,

$$< F_{pq} > \propto (\Delta X_\eta / D)^{\phi_{pq}}, \tag{3.17}$$

as $1/D$ approaches a large value.

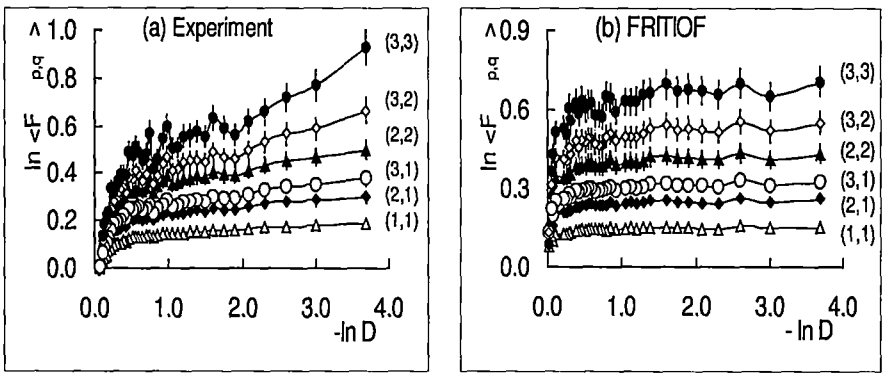

Figure 3.11: Plot showing dependence of factorial correlators of different ordered against correlation length. Points represent experimental values in η-space. In each case only the last six points have been used to fit straight lines to data and obtain the exponents. The lines are drawn to guide the eye.

In Fig. 3.11 the experimental results as well as the FRITIOF simulated results on F_{pq} in η-space, have been graphically presented for several different combinations of p and q. For each such combination the experimental points show that, as $-\ln D$ increases, there is a rapidly growing correlation at the beginning of the curve, a saturation next, and again a moderate linear rise at the end. On the other hand for the simulated event sample, with increasing $-\ln D$ hardly any variation in the values of $\ln F_{pq}$ can be found. The variation of experimental $\ln F_{pq}$ with $-\ln D$ is not linear, and the exponents ϕ_{pq} have been obtained by fitting straight lines to the data only in the large $-\ln D$ region, a region that corresponds to short range correlation. The values of ϕ_{pq} and r^2 have been incorporated in Table 3.3 for the experiment as well as for the FRITIOF simulated data. Negligibly small values of ϕ_{pq} for the simulated data shows that, the model can not reproduce the experimentally observed correlations. According to the α-model and the

log-normal approximation, the exponents should follow a relation like,

$$\phi_{pq} = \phi_{p+q} - \phi_p - \phi_q = p\,q\,\phi_{11}. \tag{3.18}$$

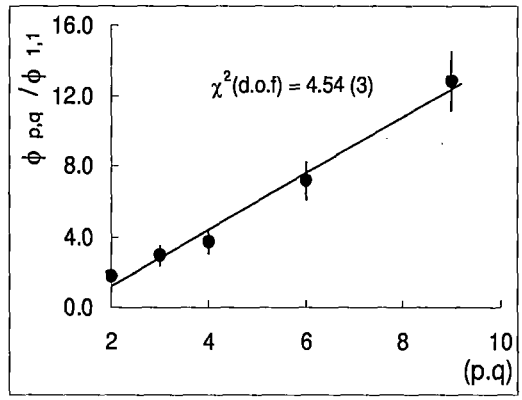

Figure 3.12: Plot of $\phi_{p,q}/\phi_{1,1}$ against $(p \cdot q)$ in η-space according to the predictions of α-model. The solid line is the best fitted straight line to the experimental values.

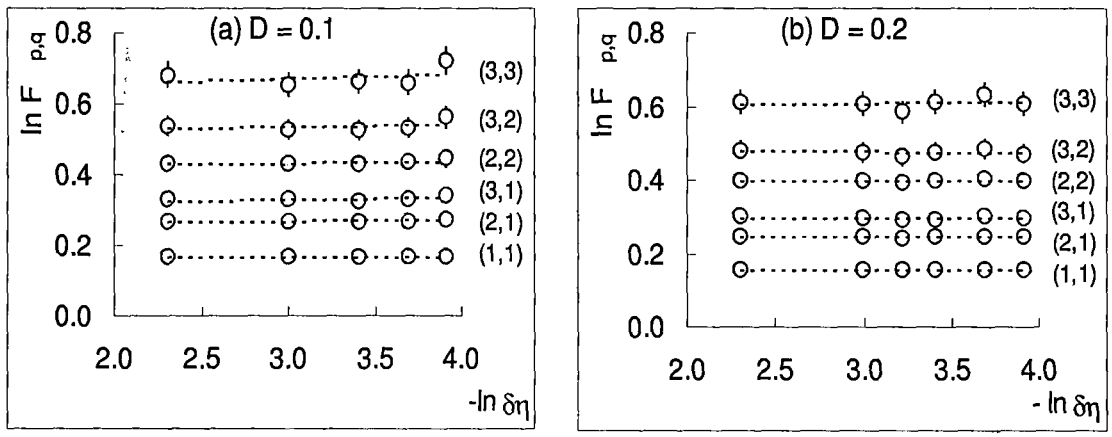

Figure 3.13: Plot showing independence of factorial correlators with respect to phase-space partition size δX_η at fixed D. The dashed lines are best fitted straight lines to the data.

The values of ϕ_{pq}/ϕ_{11} should therefore, linearly rise with the product $(p \cdot q)$. Such a plot has been given in Fig. 3.12 for the experimentally obtained values only. Another

prediction of the α-model is that, for a fixed D the correlatores should be independent of δX. This aspect can be verified from Fig. 3.13, where graphical plot of $\ln F_{pq}$ for several different values of δX_η and at a fixed $D(= 0.1,$ and $0.2)$, have been shown both for the experiment and for the FRITIOF. Within errors the δX_η independence of F_{pq} has been established. It has to be mentioned that, such a property does not only hold for the α-model, but is a feature of any model that takes short range correlation into consideration [23]. Overall, the study shows presence of short range correlation in our heavy-ion data, and gross features of the experimental observations are consistent with predictions of α-model. Most of the long range correlations have probably been smeared out due to intermixing of many sources of particle production.

Table 3.3. Values of exponents of factorial correlators of different orders both for the experiment and FRITIOF simulated events, along with the Pearson's r^2 co-efficient showing goodness of linearity.

Values of	Experiment		FRITIOF	
(p,q)	$\phi_{p,q}$	r^2	$\phi_{p,q}$	r^2
(1,1)	0.0152 ± 0.0019	0.9433	0.0047 ± 0.0012	0.6589
(2,1)	0.0272 ± 0.0038	0.9270	0.0087 ± 0.0018	0.7549
(3,1)	0.0447 ± 0.0061	0.9317	0.0126 ± 0.0028	0.8202
(2,2)	0.0562 ± 0.0066	0.9477	0.0171 ± 0.0021	0.8235
(3,2)	0.1086 ± 0.0090	0.9733	0.0291 ± 0.0044	0.8459
(3,3)	0.1946 ± 0.0096	0.9904	0.0395 ± 0.0053	0.8731

3.2.3 Oscillatory Multiplicity Moments

The effect of multiparticle correlation over and above any trivial background effect can also be studied with the help of normalized factorial cumulant moments (K_q) [24]. These moments provide a measure of genuine higher order correlation beyond the lower one, and they are defined as,

$$K_q = F_q - \sum_{j=1}^{q-1} \binom{q-1}{j-1} F_{q-j} K_j, \quad j = 2, 3, \cdots \tag{3.19}$$

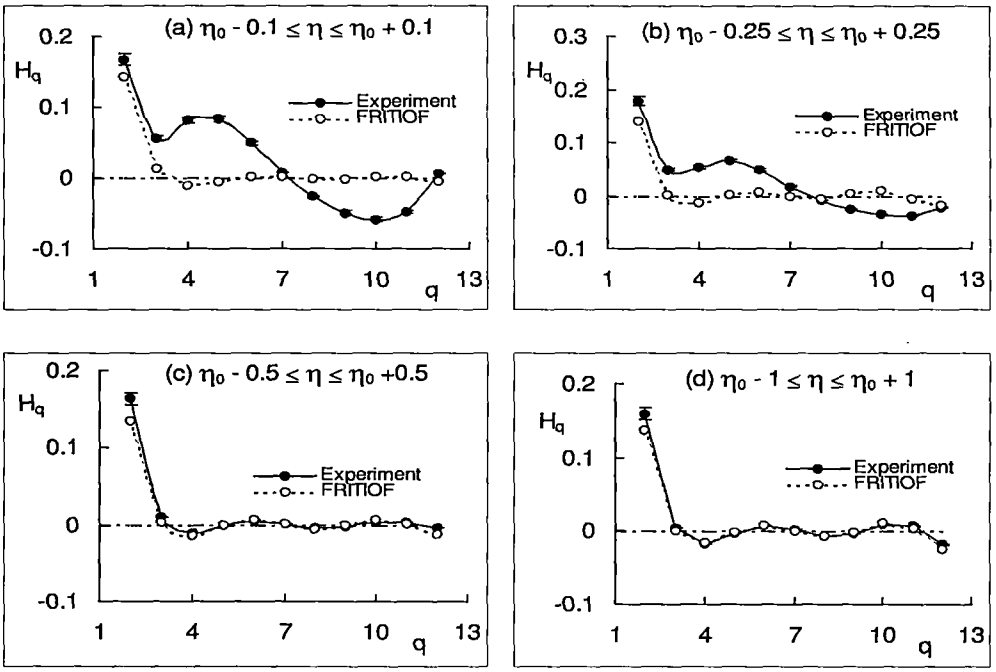

Figure 3.14: Plot of oscillatory multiplicity moments H_q against q at different η intervals indicated in the diagrams. Note how the experimental results coincide with the FRITIOF prediction with increasing η_{cut}.

For a Poisson distribution $K_1 = 1$ and $K_q = 0$ for $q > 1$. Nonzero value of K_q (for $q \geq 2$) indicates presence of two or more particle correlation in the inclusive density distribution of produced particles. It has been predicted by a parton shower cascade model based on QCD, that the K_q moments would oscillate irregularly around the zero value with increasing order q. Both F_q and K_q have strong energy and order dependence. Sometimes, a new set of normalized cumulant moments is introduced as,

$$H_q = K_q/F_q, \tag{3.20}$$

where such dependences are partially canceled. H_q reflects genuine q-particle correlation integral relative to the global correlation integral. In the cases of high-energy e^+e^-, hh and hA interactions, oscillatory behaviour of H_q with increasing q has been experimentally confirmed [25]. Whereas, for e^+e^- and hh interactions the oscillatory behavior has been attributed to the multicomponent structure of the particle production process, in the hA case the result has been explained in terms of a leading particle cascade model. In all

cases for each participating particle either a negative binomial, or a modified negative binomial multiplicity distribution, or both has been successfully used. In the present case of ^{32}S-Ag/Br interactions, the variation of H_q moments with order q has been graphically presented in Fig. 3.14, for the experiment as well as for the FRITIOF data. Several η intervals like $(\eta_0 - \eta_{cut}) \leq \eta \leq (\eta_0 + \eta_{cut})$ with $\eta_{cut} = 0.1, 0.25, 0.5$ and 1.0, each centered about η_0 have been chosen to examine the jet structure in central particle producing region. One can see that, in narrow intervals ($\eta_{cut} = 0.1, 0.25$) the experimental results are significantly different from the FRITIOF results. The extent of oscillation, particularly in the high q region is much larger for the experiment than it is for the FRITIOF. This is indicative of different characteristics of the jet structure between the experimental and simulated data. Unlike the hh and hA cases the oscillation, though present in our AB experimental result, is not always about $H_q = 0$, but in the small q (< 7) region it is above the $H_q = 0$ line. The FRITIOF on the other hand exhibits only a small oscillation with increasing q. As the η interval size is increased, at ($\eta_{cut} = 0.5$, and 1.0) probably due to intermixing from different particle producing regions, the correlation effects are washed out, and the experimental result starts to coincide with the simulated result showing only a little or no oscillation. Only a sharp fall around $q = 2 - 4$ is prominently visible in each of these diagrams.

3.3 Discussion

An analysis of spatial distribution of shower tracks in central and semicentral ^{32}S-Ag/Br interactions at 200A GeV/c has been presented above. Multiplicity moments related to the intermittency phenomenon, with varying phase-space interval size have been evaluated. The results show presence of weak intermittency in the one dimensional distributions of singly charged produced particles. The intermittency results however, are not independent of the choice of phase-space variable. Even the weak intermittency effect in η-space can not be explained with the Lund Monte Carlo code FRITIOF, and in the φ-space the same could not be reproduced by assuming independent emission of particles based on random number generation. Fluctuations in the density distribution of like sign charged particles in small intervals of phase-space can be explained in terms of Bose-Einstein (BE)

correlation, i.e., interference among identical particles emitted by an extended coherent source. For shower tracks, created by both positive and negative charges (mostly pions), the increase of SFM with decreasing interval size shows a small but significant effect beyond the BE correlation effect. Lower value of intermittency indexes in experiments involving higher mass number or energy of the incident nucleus have been explained in terms of intermixing of more sources of particle production within the collision region. A close scrutiny of the experimentally obtained ϕ_q values does not allow us to draw any strong conclusion regarding any definite mechanism underlying the observed weak intermittency effect. On the one hand, absence of any noticeable prominent minimum in the λ_q vs. q plot does not necessarily indicate that, there exist a mixture of two phases - one normal with a large number of small peaks and shallow dips, and the other a spin glass with a small number of sharps peaks and deep valleys. Thus the present observation hardly corroborates the proposition that, the observed intermittency effect results due to presence of a mixture of two states like those mentioned above, as has been suggested and observed in the JINR data [27]. On the other hand, the Ginzburg-Landau parameter $\nu = 1.327 \pm 0.009$ with some degree of uncertainty in its error, is different from the universal value $\nu = 1.304$ necessary for a second order QCD phase transition to take place. Even if there is any phase transition, in the present case it has to be non-thermal type as a greater than unity Levy index ($\mu = 1.1$) indicates. However, a hierarchical relation between the SFMs has been established, that indicates some kind of interdependence between the correlation functions of different order. Also a multifractal structure of the particle density function in 1-d has also been established from the study of the anomalous dimensions [26].

Intermittency analysis in 2-d shows much stronger effect with an upward nonlinear bending in the SFM variation with decreasing interval size. The 2-d result confirms that in 1-d, intermittency effect is substantially shadowed due to projection effect. In the midst of all confusion regarding the exact reason, probably a scale invariant cascade mechanism in 2-d remains the only viable alternative as responsible for the intermittency phenomenon in the present case. An anisotropy between the phase-space distributions along longitudinal (η) and transverse (φ) directions has been found in our data. This lead us to conclude that, the intermittency is a result of self-affinity rather than a self-similarity in the par-

ticle distribution. Study of factorial correlators shows presence short range bin to bin correlation, that is consistent with the predictions of a simple α-model. Once again the observed correlation could not be accounted for by the FRITIOF prediction. Result on oscillatory multiplicity moments (H_q) confirms presence of true higher order ($q \geq 2$) correlation in our ^{32}S-Ag/Br data, that can not be reproduced by the FRITIOF. It also shows that, such correlation effects are more prominent in narrow phase-space intervals. With growing phase-space interval size the correlation effects are neutralized, and ultimately the experimental results coincide with the FRITIOF simulated results.

Bibliography

[1] A. Bialas and R. Peschanski, *Nucl. Phys.* **B 273**, 703 (1986)
A. Bialas and R. Peschanski, *Nucl. Phys.* **B 308**, 857 (1988).

[2] JACEE Collaboration, T.Burnett *et al.*, *Phys. Rev. Lett.* **50**, 2062 (1983).

[3] E. A. De Wolf, I. M. Dremin, and W. Kittel, *Phys. Rep.* **270**, 1 (1996)
W. Kittel and E. A. De Wolf, *Soft Multihadron Dynamics*, (World Scientific, Singapore, 2005).

[4] B. Andersson, G. Gustafson, and B. Nilsson-Almqvist, *Nucl. Phys.* **B 281**, 289 (1987).
B. Nilsson-Almquist and E. Stenlund, *Comp. Phys. Commun.* **43**, 387 (1987).

[5] K. Fialkowski *et al.*, *Acta Phys. Pol.* **B 20**, 639 (1989).

[6] A. Bialas and M. Gazdzicki, *Phys. Lett.* **B 252**, 483 (1990).

[7] I. V. Ajinenko *et al.*, *Phys. Lett.* **B 222**, 306 (1989)
N. M. Agababyan, *et al.*, *Phys. lett.* **B 382**, 305 (1996).

[8] M. R. Spiegel *Theory and Problems of Statistics*, (McGraw-Hill Book Co., UK, 1988).

[9] EMU01 Collaboration, M. I. Adamovich *et al.*, *Nucl. Phys.* **B 388**, 3 (1992).

[10] B. Buschbeck, R. Lipa and R. Peschanski, *Phys. Lett.* **B 215,** 788 (1988)
W. Braunscheweig *et al.*, *Phys. Lett.* **B 231**, 548 (1988)
I. Derado, G. Jansco, N. Schmitz and P. Stopa *Z. Phys.* **C 47,** 23 (1990)

[11] KLM Collaboration, R. Holynski *et al.*, *Phys. Rev. Lett.* **62**, 733 (1989)
KLM Collaboration, R. Holynski *et al.*, *Phys. Rev.* **C 40**, 2449 (1989)
EMU01 Collaboration, M. I. Adamovich *et al.*, *Phys. Rev. Lett.* **263**, 539 (1991).

[12] W. Ochs, *Phys. Lett.* **B 247**, 101 (1990)
W. Ochs, *Z. Phys.* **C 50**, 339 (1991).

[13] S. V. Chekanov and V. I. Kuvshinov, *Acta Phys. Pol.* **B 25**, 1189 (1994).

[14] Ph. Brax and R. Peschanski, *Phys. Lett.* **B 253**, 225 (1991).

[15] R. C. Hwa and M. T. Nazirov, *Phys. Rev. Lett.* **69**, 741 (1992).

[16] A. Bialas and K. Zalewski, *Phys. Lett.* **B 238**, 413 (1990).

[17] L. Van Hove, *Phys. Lett.* **B 28**, 429 (1969).

[18] Y. Wu and L. Liu, *Phys. Rev. Lett.* **70**, 3197 (1993).

[19] L. Liu, Y. Zhang and Y. Wu, *Z. Phys.* **C 69**, 323 (1996).

[20] C. Gang, L. Liu and G. Yanmin, arxiv:hep-ph/9812329v1 (1998).

[21] EMU01 Collaboration, M. I. Adamovich *et al.*, *Z. Phys.* **C 76**, 659 (1997).

[22] NA22 Collaboration, V. V. Aivazyan *et al.*, *Phys. Lett.* **B 258,** 487 (1991).
EMC Collaboration, I. Derado *et al.*, *Z. Phys.* **C 54,** 357 (1992).
D. Ghosh *et al.*, *Phys. Rev.* **C 52,** 2092 (1995).

[23] E. A. De Wolf, *Proceedings of the Ringberg Workshop on Multiparticle Production* eds. Hwa R C *et al.*, 222 (World Scientific, Singapore, 1992)

[24] P. Carruthers, H. C. Eggers and I. Sarcevic, *Phys. Lett.* **B 254**, 258 (1991).
P. Carruthers, H. C. Eggers and I. Sarcevic, *Phys. Rev.* **C 44**, 1629 (1991).

[25] I. M. Dremin, *Phys. Lett.* **B 313**, 209 (1993)
N. Suzuki, M. Biyajima, G. Wilk and Z. Wlodarczyk, *Phys. Rev.* **C 58**, 1720 (1998).

[26] M. K. Ghosh, A. Mukhopadhyay and G. Singh, *J. Phys.*, **G 32,** 2293 (2006).

[27] E. K. Sarkisyan, L. K. Gelovani, G. L. Gogiberidze, and G. G. Taran, *Phys. Lett.* **B 347,** 439 (1995).